Environmental Earth Sciences (2025) 84:222
https://doi.org/10.1007/s12665-025-12216-1

ORIGINAL ARTICLE

Spatio-temporal evaluation of ionospheric disturbances before, during and after earthquakes using differential rate of TEC (DROT) from GPS measurements

Secil Karatay[1] · Feza Arikan[2] · Atinc Pirti[3]

Received: 29 July 2024 / Accepted: 22 March 2025 / Published online: 15 April 2025

Abstract
This study presents a comprehensive spatio-temporal analysis of ionospheric disturbances associated with seismic activity by applying the Differential Rate Of TEC (DROT) algorithm to GPS-based Total Electron Content (TEC) data. The investigation covers ten major earthquakes (Mw 9.0–5.6), examining ionospheric variability across pre-seismic, co-seismic, and post-seismic periods, alongside geomagnetically quiet and disturbed days. Results reveal that ionospheric perturbations are not confined to the pre-earthquake phase; significant anomalies are also observed during and up to six days after the seismic events. On earthquake days, DROT values predominantly cluster between 60 and 70%, indicating large-scale disturbances, while medium-scale disturbances (50–60%) are prevalent in the days leading up to and following the earthquakes. Spatial analysis shows stronger disturbances within 500 km of epicenters, diminishing with distance. The findings support the Lithosphere-Atmosphere-Ionosphere Coupling (LAIC) model, highlighting the sustained influence of seismic processes on the ionosphere. By distinguishing between seismically and geomagnetically induced disturbances, this study underscores the potential of DROT as a tool for real-time ionospheric monitoring and contributes to efforts in earthquake precursor detection and early warning systems.

Keywords Ionospheric disturbances · Earthquake precursors · Total Electron content (TEC) · Differential rate of TEC (DROT) · Spatio-Temporal analysis

Introduction

The intricate movements of tectonic plates and the Earth's crust form the basis of the complex nature of earthquakes. Faults that rupture before to earthquakes impact multiple physical systems that in turn influence the overall seismic event. The lithosphere, atmosphere, hydrosphere and ionosphere make up this multiple physical systems that they can all interact in different ways in the build-up to an earthquake. The main process is the build-up and abrupt release of stress along the fault line. Many physical mechanisms, such as Radon emission and electromagnetic changes, are significantly affected and changed when faults rupture before an earthquake. Rock fractures can cause the atmosphere to fill with gasses such as Radon (Pulinets & Ouzounov, 2011; Trique et al. 1999; King 1986; Igarashi et al. 1995). Certain earthquakes have been shown to be preceded by elevated Radon levels that may indicate subsurface condition changes (Khan et al. 2021). Fault-related stress and strain may have an impact on Earth's electromagnetic field and cause ionospheric anomalies and disturbances that can be observed by satellites and ground-based sensors (Karatay et al. 2010; Gurbuz et al. 2023; Ghimire and Chapagain 2022; Tachema 2024). A topic of great scientific interest is the association between pre-earthquake ionospheric anomalies and seismic activity, since these anomalies may act as precursors to possible earthquakes. Some ionospheric

✉ Secil Karatay
skaratay@kastamonu.edu.tr

1 Department of Electrical-Electronics Engineering, Kastamonu University, Kuzeykent, Kastamonu 37150, Türkiye

2 Department of Electrical and Electronics Engineering, Hacettepe University, Beytepe, Ankara 06800, Türkiye

3 Department of Geomatic Engineering, Yıldız Technical University, Esenler, Istanbul 34220, Türkiye

anomalies and disturbances, such as variations in temperature and electron density and Total Electron Content (TEC), have been detected before the seismic activity (Karatay et al. 2010; Pulinets et al. 2004, 2005; Carbone et al. 2021; Budak et al. 2024; Nayak et al. 2023). These anomalies are believed to be caused by the transmission of seismic waves that alter the Earth's magnetic field or by the discharge of gases from the Earth's crust, such as Radon, which ionizes the atmosphere (Larkina et al. 1989; Bolt 1964; Donn and Posmentier 1964; Hirshberg et al. 1967; Khan et al. 2021; Su and Chen 2023; Tsuchiya et al. 2024). These ionospheric anomalies and disturbances have been detected by satellite-based observations and ground-based monitoring stations hours to days ahead of major earthquakes, suggesting a potential connection between the building of subterranean stress and ionospheric responses.

Spatio-temporal analysis of the pre-earthquake disturbances in the ionosphere is important to comprehend and foresee the seismic events. Variations in TEC (Karatay et al. 2010), electromagnetic emissions (Molchanov et al. 1995) and plasma density (Tao et al. 2017) are examples of ionospheric disturbances that are frequently detected days to hours before to significant earthquakes. These investigations shed light on the temporal evolution and spatial extent of these disturbances. These disturbances can be identified and the accuracy precursor detection can be improved by mapping these ionospheric disturbances and anomalies over time and comparing them to seismic activity (Yao et al. 2012; Hirooka et al. 2011; Xie et al. 2021; Liu et al. 2023). It helps differentiate earthquake-related disturbances from other ionospheric phenomena like geomagnetic storms or solar flares. Furthermore, the integration of multi-source data from satellites, ground-based sensors, and global positioning systems is made possible by spatio-temporal studies, providing a thorough understanding of the interaction between the lithosphere, atmosphere and ionosphere (Pulinets & Ouzounov, 2011). Development of the predictive models, improvement of the early warning systems and mitigation of the risks for large-scale seismic disasters all depend on such thorough investigations.

Ionosphere is a layer of Earth's upper atmosphere that lies between 60 and 1000 km above the surface that is made up by ionized particles produced by solar radiation. Because of this ionization and ionosphere's ability to reflect and refract radio waves, it is important to satellite and radio communications. The ionosphere significantly varies depending on time of day, geographic location, seasons, solar, geomagnetic activities, and to a lesser extent, seismic activities, also including well-documented co-seismic effects and potential pre-seismic anomalies under investigation. The Total Electron Content (TEC), a measure of the total number of electrons in an ionosphere column with a cross-sectional area of one square meter, is a crucial quantity for comprehending the ionosphere's effect on radio and satellite communication technology. Increases in TEC values might result in signal delays and inaccuracies in navigation and positioning applications. Reliable communication and navigation systems are ensured by the ongoing monitoring of TEC which aids in prediction and mitigation of such impacts. TEC also varies depending on solar activity, time of day, season, geographic location, solar, geomagnetic and seismic activities (Davies 1990; Hargreaves 1992; Kelley 1989). This field of study makes use of information from space-based instruments and ground-based receivers to increase satellite-based technology reliability and our comprehension of ionospheric dynamics. The unit of TEC is TECU, where one TECU is equal to 10^{16} el/m^2. With its global network of sensors, the Global Positioning System (GPS) offers an affordable way to monitor ionospheric variability over a substantial area of the global landmass and estimate TEC (GPS-TEC) (Arikan et al. 2003; Nayir et al. 2007; Sezen et al. 2013).

In recent years, extensive research has been presented in the literature on the Lithosphere-Atmosphere-Ionosphere Coupling (LAIC) model, which describes the coupling between seismic activity and the ionosphere's electromagnetic state (Pulinets & Ouzounov, 2011; Hayakawa et al. 2021; Molchanov et al. 2004). Numerous studies have demonstrated that earthquakes can induce perturbations and disturbances in the ionospheric plasma. These perturbations and disturbances, which can occur both before and after seismic events, are frequently detected as anomalies in Total Electron Content (TEC) (Pulinets and Boyarchuk 2004; Liu et al. 2000; Krankowski et al. 2006; Karatay et al. 2010). These studies have indicate that earthquakes can induce perturbations and disturbances in the ionospheric plasma. These perturbation and disturbances can occur before or after seismic events and are frequently detected as anomalies in TEC. Ionospheric disturbances are thought to be caused by atmospheric disturbances that propagate upward and generate acoustic waves(Weaver et al. 1970) and gravity waves(Row 1966) as a result of the ground motion. During seismic activity, electric fields caused by stress and strain in the Earth's crust may have an impact on the ionosphere (Pulinets et al. 1998; Ghosh et al. 2009). Early warning systems and earthquake prediction may be possible by detecting these ionospheric anomalies through GPS-based TEC measurements and other ionospheric monitoring methods (Pulinets and Boyarchuk 2004; Liu et al. 2000; Shah et al. 2020). Most analytical research investigating the seismo-ionospheric relation has employed statistical methods. The objective of these investigations has been to identify statistical relationships between ionospheric parameters, including TEC and the critical frequency of the ionospheric F2-region (Pulinets et al. 2004; Karatay et al. 2010; Liu et al. 2004a;

Kouris et al. 2006; Davidenko and Pulinets 2019; Colonna et al. 2023). The detection and classification of anomalous ionospheric signals during geomagnetic and seismic activity remain challenging and require the application of sophisticated signal processing techniques. Recently, strong Machine Learning (ML) algorithms have been developed that can handle data that increases logarithmically with power hardware. The ML algorithms have been applied to GPS-TEC measurements, ionosondes and satellite observations to classify, detect and predict the possible earthquake precursor signals and geomagnetic disturbances in the ionosphere in the recent studies in the literature (Akyol et al. 2020; Budak et al. 2024; Karatay and Gul 2023; Budak and Gider 2023; Eshkuvatov et al. 2023). These algorithms include noise filtering, data normalization, and the identification of critical markers of ionospheric disturbances, like abrupt shifts in TEC values, amplitude variations in signals, or phase fluctuations. Real-time ionospheric monitoring can also be facilitated by the deployment of ML algorithms, which offer alerts and ongoing analysis upon detection of possible precursor signals for earthquakes.

Rate Of TEC (ROT), an additional highly effective approach for identifying ionospheric disturbances, is equivalent to the time derivative of phase-leveled TEC over a one-minute duration (Pi et al. 1997; Krankowski et al. 2006). Another common way to represent the rate of variation of TEC is the Rate Of TEC Index (ROTI) that is the standard deviation of ROT (Basu et al. 1999). Spatio-temporal maps derived from ROTI have been used to show the location and intensity of ionospheric disturbances (Cherniak et al. 2014). It can be said that it is very difficult to automatically detect the disturbance caused by ionosphere fluctuation since ROT on TEC has trouble from mapping function inaccuracies and produces extremely noisy values. Differential Rate Of TEC (DROT), an algorithm derived from ROT is the ratio of the ROT's metric norm to the metric norm of the difference between the ROT and the trend. According to published researches in the literature (Efendi and Arikan 2017; Koroglu and Arikan 2018a, b, 2020; Karatay 2020; Arikan et al. 2017), the DROT technique offers a quick way to identify potential ionospheric disturbances and a scale for their intensity. In this study, DROT is applied to GPS-TEC data to evaluate the pre-earthquake disturbances in the ionosphere. DROT is also applied to geomagnetically disturbed and quiet days data to characterize the seismic and geomagnetic disturbances. A brief discussion of the DROT algorithm is given in Sect. The data and the method. The results of applying the DROT algorithm to the GPS-TEC data obtained for geomagnetically disturbed and quiet days and ten earthquake periods with magnitude greater than Mw 5 are presented in Sect. Results and discussion.

The data and the method

The Regularized Estimation of TEC (Reg-Est) algorithm using dual-frequency Continuously Operating Reference Stations (CORS) is used in this study to compute IONOLAB-TEC as given in Arikan et al. (2003) and Arikan et al. (2004). The IONOLAB-TEC uses the state-of-the-art Reg-Est algorithm for signal processing to integrate all usable satellites over the local horizon of the GPS receiver (Arikan et al. 2003, 2004; Nayir et al. 2007; Sezen et al. 2013). The satellite Differential Code Biases (DCBs) are derived from IONEX files and the receiver DCBs are calculated using the IONOLAB-BIAS algorithm (Arikan et al. 2008). The IONEX files, satellite ephemeris and satellite DCB are obtained from http://ftp.cddis.gsfc.nasa.gov/gps/products/ionex/. In this study, IONOLAB-TEC is estimated as 576 values with 2.5 min resolution for a single station in a day. The Differential Rate Of TEC (DROT) algorithm, which will be explained below, is applied to the IONOLAB-TEC data estimated for each Global Navigation Satellite Systems (GNSS) station demonstrated in Fig. 1 during the ten earthquake periods given in Table 1. The earthquakes given in Table 1 are listed according to their magnitude. The information of the earthquake days are obtained from https://earthquake.usgs.gov/earthquakes.

IONOLAB-TEC is estimated for five days before the earthquakes and the earthquake days (pre-seismic and co-seismic period) and six days after the earthquakes (post-seismic period) for each station presented in Table 1; Fig. 1. Additionally, IONOLAB-TEC is also estimated for each station for the most disturbed and quiet days in each earthquake year (geomagneticaly disturbed and quiet periods). The investigation periods are presented in Table 2. Kp, Ap and Dst values for disturbed and quiet periods are given in Fig. 2. The indices in Fig. 2 are obtained from Space Weather Prediction Center (NOAA) at http://ftp.swpc.noaa.gov/pub/indices/old_indices/ and World Data Center for Geomagnetism (WDC) at http://wdc.kugi.kyoto-u.ac.jp/dstdir/.

The ionosphere is comparatively less disturbed in the days before the earthquakes in all chosen earthquake periods compared to geomagnetically active days. While the days selected as "quiet days" may include Kp values up to 5.6, it is acknowledged that these values correspond to 'minor geomagnetic activity' as per NOAA's Space Weather Scale. For this study, quiet days are defined relative to the geomagnetic activity levels observed in other periods within the same dataset. The maximum values of Kp and Ap indices are 5.6 and 67, respectively and the maximum Dst index reaches −67 nT. This classification ensured that the selected days represent the least geomagnetically influenced periods,

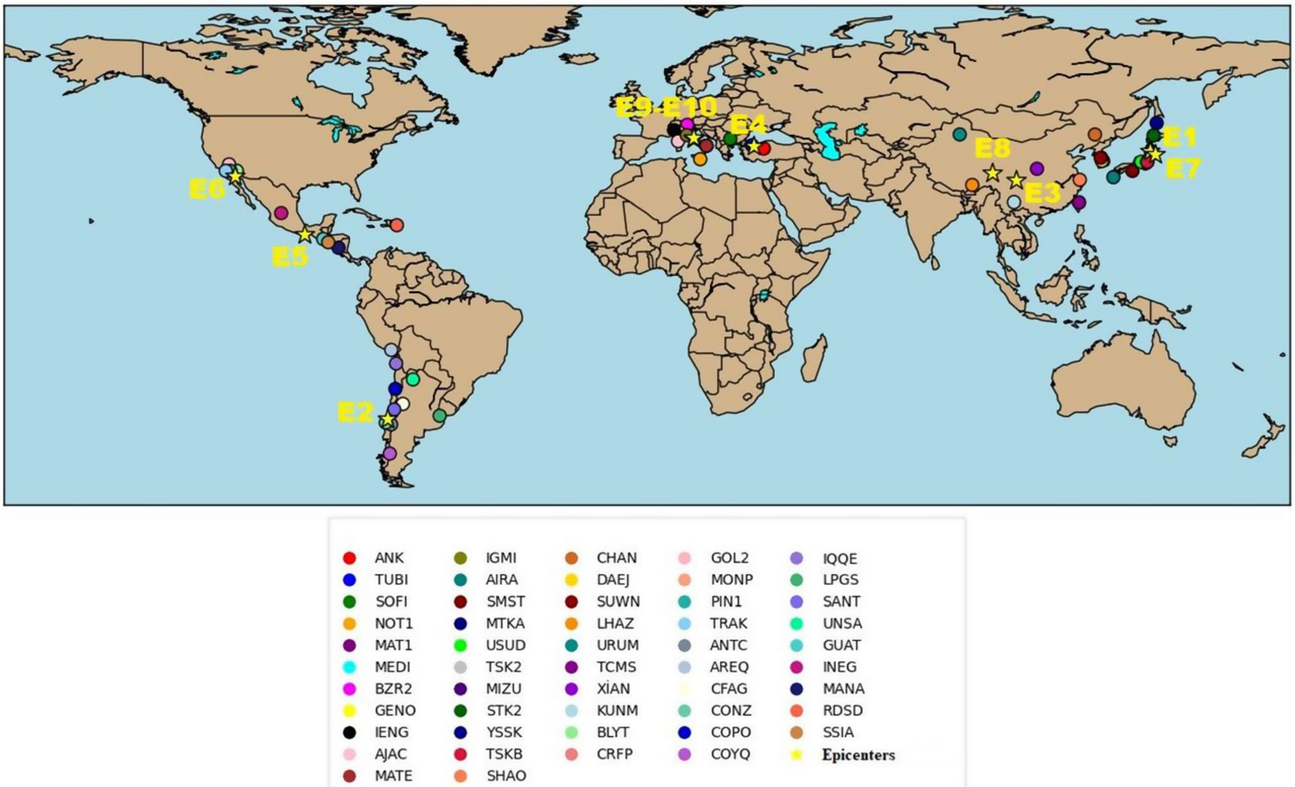

Fig. 1 Location of GNSS stations used in the study and the epicenters

aiding in isolating ionospheric disturbances potentially related to seismic activity. (GFZ, n.d.).

TEC data of length N is represented with vector $\boldsymbol{x}_{u;d}$ for day d of any GPS receiver u in the following way:

$$\boldsymbol{x}_{u;d} = [x_{u;d}(1) \ldots \ldots x_{u;d}(n) \ldots \ldots x_{u;d}(N)]^T \tag{1}$$

where $1 \leq n \leq N$, n is the time index and T is the transpose operator. One of the most used techniques for examining the temporal variability of the ionosphere is the Rate of TEC (ROT). ROT is measured in TECU/s and is equal to the rate of change of TEC during a given time period (Carmo et al. 2021; Wilken et al. 2018; He et al. 2023). The temporal derivative vector, or ROT ($\boldsymbol{R}_{u;d}$), is calculated using TEC data in this study in the following way:

$$R_{u;d}(n) = \frac{x_{u;d}(n+1) - x_{u;d}(n)}{\Delta t} \tag{2}$$

Δt is $2.5 \times 60 = 150\, s$ in the above equation. In this study, the trend structure for TEC is removed using two sliding window median filters of lengths T_{f1} and T_{f2}, as explained in Karatay (2020). By applying two sliding window median filters, median filtered ROTs are obtained as $\boldsymbol{Y}_{u;d}$ and $\widehat{\boldsymbol{Y}}_{u;d}$ vectors with T_{f1} and T_{f2}, respectively. T_{f1} and T_{f2} correspond to 12.5 min and 4.2 h with 5 and 101samples, respectively. The difference vector between $\boldsymbol{Y}_{u;d}$ and $\widehat{\boldsymbol{Y}}_{u;d}$ is obtained as follow:

$$\boldsymbol{D}_{u;d=}\boldsymbol{Y}_{u;d} - \widehat{\boldsymbol{Y}}_{u;d} \tag{3}$$

The degree of variation between ROT and its trend can be defined with Differential Rate Of TEC (DROT) (Efendi and Arikan 2017; Koroglu and Arikan 2018a, b, 2020; Karatay 2020). DROT has percentage values between 0 and 100. An ionospheric disturbance causes a rise in deviation from the trend; hence, DROT increases in direct proportion to the strength of the disturbance or plasma irregularity. The ratio of the difference between the smoothed ROT, $\boldsymbol{Y}_{u;d}$ and $\boldsymbol{D}_{u;d}$ are used to calculate DROT values as follows:

$$DROT_{u;d} = \frac{\sqrt{\sum_{n=1}^{N}[D_{u;d}(n)]^2}}{\sqrt{\sum_{n=1}^{N}[Y_{u;d}(n)]^2}} x100 \tag{4}$$

As a result, the DROT values increase in proportion to the strength of the difference vector $\boldsymbol{D}_{u;d}$ depending on an increase in variability relative to the background ionosphere. An operating chart of the DROT algorithm is given in Fig. 3.

Table 1 Geographic location, time, magnitude and depth of the chosen earthquakes and used GNSS station (USGS, n.d.)

Earthquake (Number: Location)	Time (Day, UTC Time)	Epicenter (Latitude-Longitude)	Magnitude (Richter Mw)	Depth (km)	Stations
E1: Tohoku, Japan	11 March 2011 UTC: 05:46	38.32°N-142.36°E	9.0	29	AIRA, MTKA, MIZU, SMST, TSK2, TSKB, STK2, USUD, YSSK
E2: Maule, Chile	27 February 2010 UTC: 06:34	35.84°S-72.71°W	8.8	35	ANTC, AREQ, CFAG, CONZ, COPO, COYQ, IQQE, LPGS, SANT, UNSA
E3: Wench-uan, China	12 May 2008 UTC: 06:28	31.02°N-103.36°E	7.9	19	CHAN, DAEJ, GUAO, KUNM, LHAZ, SHAO, SUWN, TCMS, XIAN
E4: Golcuk, Turkiye	17 August 1999 UTC: 00:01	40.74°N-29.86°E	7.6	17	ANKR, SOFI, TUBI
E5: Oaxaca, Mexican	23 June 2020 UTC: 15:29	15.93°N-95.93°W	7.4	20	GUAT, INEG, MANA, RDSD, SSIA,
E6: Califor-nia, USA	04 April 2010 UTC :22:40	32.13°N-115.30°W	7.2	10	BLYT, CRFP, DHLG, GOL2, MONP, PIN1, TRAK
E7: Iwate, Japan	13 June 2008 UTC: 23:43	39.01°N-140.52°E	6.9	8	AIRA, MTKA, MIZU, SMST, TSK2, TSKB, STK2, USUD, YSSK
E8: Yushu, China	14 April 2010 UTC: 23:49	33.16°N-96.62°E	6.9	17	CHAN, DAEJ, GUAO, KUNM, LHAZ, SHAO, SUWN, TCMS, XIAN
E9-E10: Nor-cia, Italy	24 August 2016 UTC: 01:36−02:33	42.71°N-13.17°E 42.79°N-13.15°E	6.2 5.6	10 10	BZRG, GENO, IENG, IGMİ, MAT1, MATE, MEDI

Table 2 Earthquake, disturbed and quiet periods used in the study

	Pre-seismic and co-seismic period	Post-seismic period	Disturbed period	Quiet period
E1	06–11 March 2011	12–17 March 2011	05 August 2011	26 May 2011
E2	22–27 February 2010	28 Febru-ary-05 March 2010	05 April 2010	08 May 2010
E3	07–12 May 2008	13–18 May 2008	27 March 2008	01 January 2008
E4	12–17 August 1999	18–23 August 1999	22 October 1999	25 Septem-ber 1999
E5	18–23 June 2020	24–29 June 2020	28 Septem-ber 2020	02 March 2020
E6	30-March-04 April 2010	05–10 April 2010	05 April 2010	04 March 2010
E7	08–13 June 2008	14–19 June 2008	04 Septem-ber 2008	20 Septem-ber 2008
E8	09–14 April 2010	15–20 April 2010	05 April 2010	08 May 2010
E9				
E10	19–24 August 2016	25–30 August 2016	02 Septem-ber 2016	06 Novem-ber 2016

Efendi and Arikan (2017), Karatay (2020) and Koroglu and Arikan (2020) have used synthetic oscillations with additional amplitude, frequency, and duration on the background STEC and TEC to calibrate the intensity of ionospheric variability into three classes. The DROT value levels have been used to categorize the intensity of the ionospheric disturbances in these studies. In the aforementioned studies, medium-scale geomagnetic disturbances up to 5 TECU in magnitude are associated with disturbances corresponding to $50\% < DROT < 70\%$. Moreover, large-scale disturbances up to 5 TECU in magnitude are associated with $DROT > 70\%$. In this study, DROT values are considered in three categories as in the studies mentioned above, and ionospheric pre-earthquake disturbances are evaluated in this context.

Results and discussion

In this study, geomagnetic and seismic disturbance precursor signals are sought by using the DROT algorithm (described in Sect. 2) to IONOLAB-TEC data. The DROT algorithm is applied to IONOLAB-TEC using the several GPS stations listed in Table 1; Fig. 1 on known days of seismic and geomagnetic disturbances. The earthquake periods include ten major earthquakes with magnitude between Mw 9.0 and 5.6 as given in Table 1. The DROT algorithm is also applied for geomagnetically quiet and disturbed periods in order to distinguish seismic disturbance from geomagnetic disturbance. In order to estimate the level of the disturbance on a disturbed day, eight and seven days are

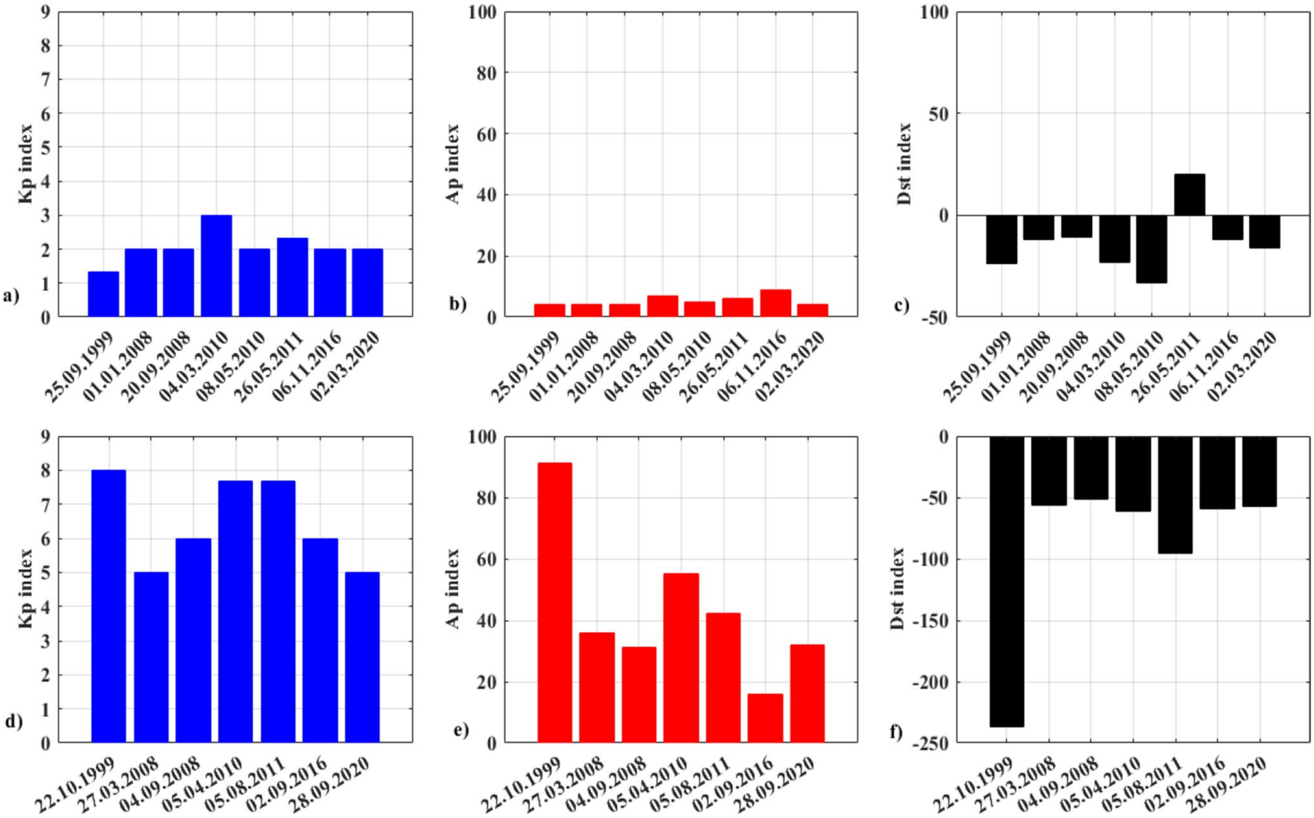

Fig. 2 Geomagnetic indices **a**) Kp indices, **b**) Ap indices and **c**) Dst indices for geomagnetically quiet days and **d**) Kp indices, **e**) Ap indices and **f**) Dst indices for geomagnetically disturbed days (NOAA, n.d.; WDC, n.d.)

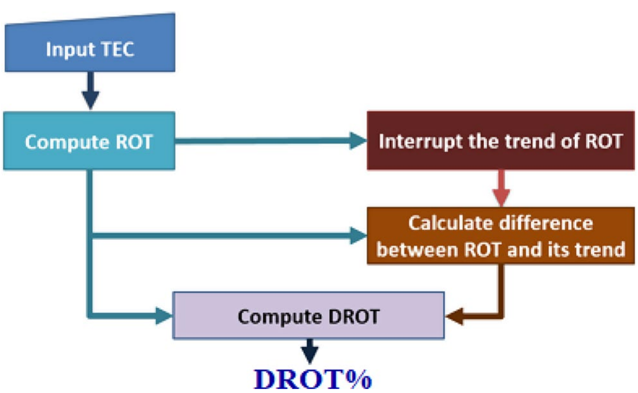

Fig. 3 Flowchart of DROT algorithm

chosen as geomagnetically quiet and disturbed days, respectively. The geomagnetic disturbed days are chosen as those with the largest Kp index in the year in which each earthquake occurred. For the purpose of this study, quiet periods were defined as days with a maximum Kp index of up to 5.6. While NOAA's Space Weather Scale defines Kp = 5 as 'minor geomagnetic activity,' these days are chosen as the least geomagnetically disturbed in comparison to disturbed periods where Kp values exceeded 6. This approach has aimed to minimize the influence of geomagnetic activity and focus on isolating seismic-related ionospheric anomalies.

This study aims to evaluate spatio-temporal pre-seismic variability of the ionosphere prior to ten significant earthquakes. The DROT algorithm is applied to IONOLAB-TEC throughout the entire day for all stations and for all days before each ten earthquakes and during geomagnetic and quiet days. Experimental Probability Density Functions (EPDFs) are obtained by grouping the DROT values into area normalized bins. The DROT values (%) for all 51 stations, eight quiet days (Fig. 4a) and seven disturbed days (Fig. 4b) are displayed as an EPDF in Fig. 4. When both figures are compared with each other, it is observed that the highest accumulation in Fig. 4a is between 45% and 50% while the highest accumulations are between 70% and 80% in Fig. 4b. The algorithm detects the oscillations in the geomagnetically disturbed periods which are an indicator of large-scale disturbances according to Efendi and Arikan (2017), Koroglu and Arikan (2018a, b) and Karatay (2020).

In Fig. 5, the EPDFs of the DROT (%) are given according to the magnitude of the earthquakes sorted from largest to smallest for six days in the chosen earthquake periods which are also given in Fig. 6. Looking at Fig. 5, it is observed that the highest accumulation for all earthquakes is between 40% and 70%. While the highest accumulation range in the largest magnitude earthquake Mw 9.0 E1 is

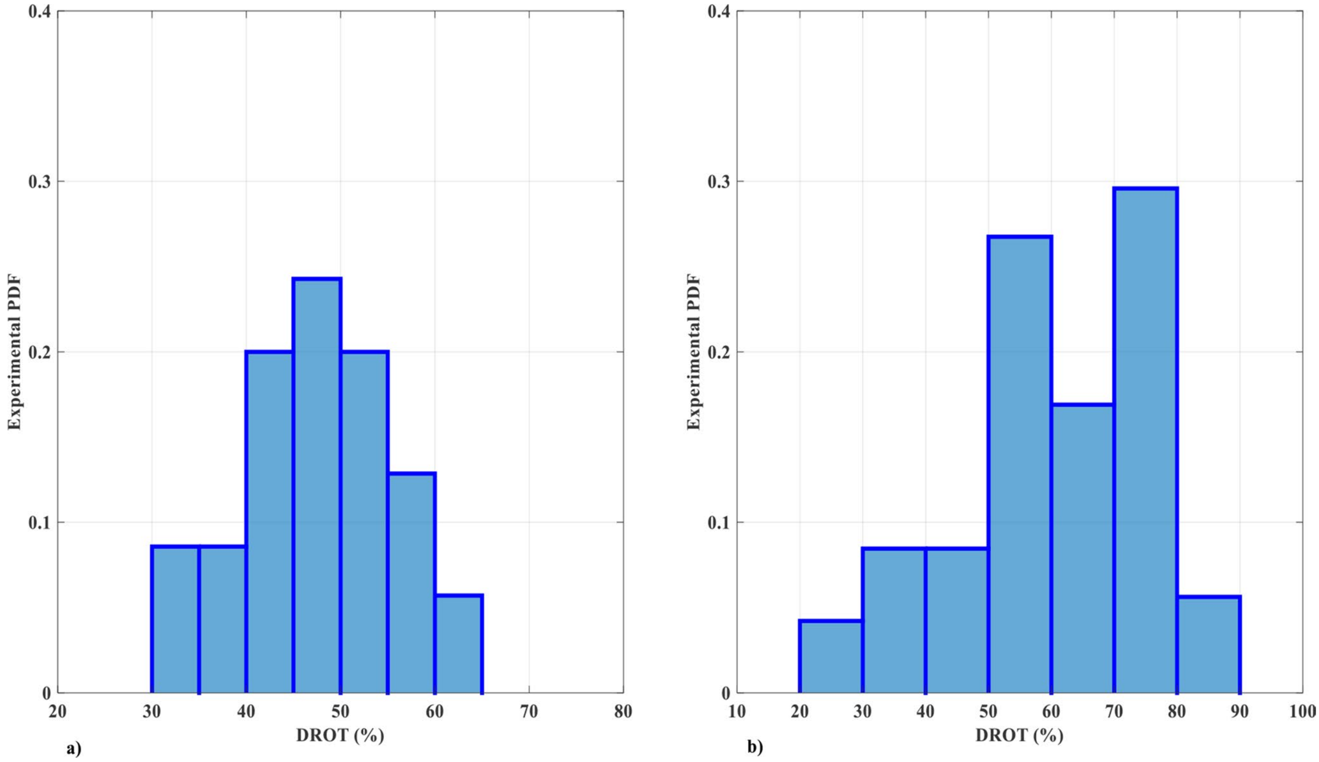

Fig. 4 The EPDFs of the DROT (%) for all stations: **a**) during geomagnetically quiet days and **b**) during geomagnetically disturbed days

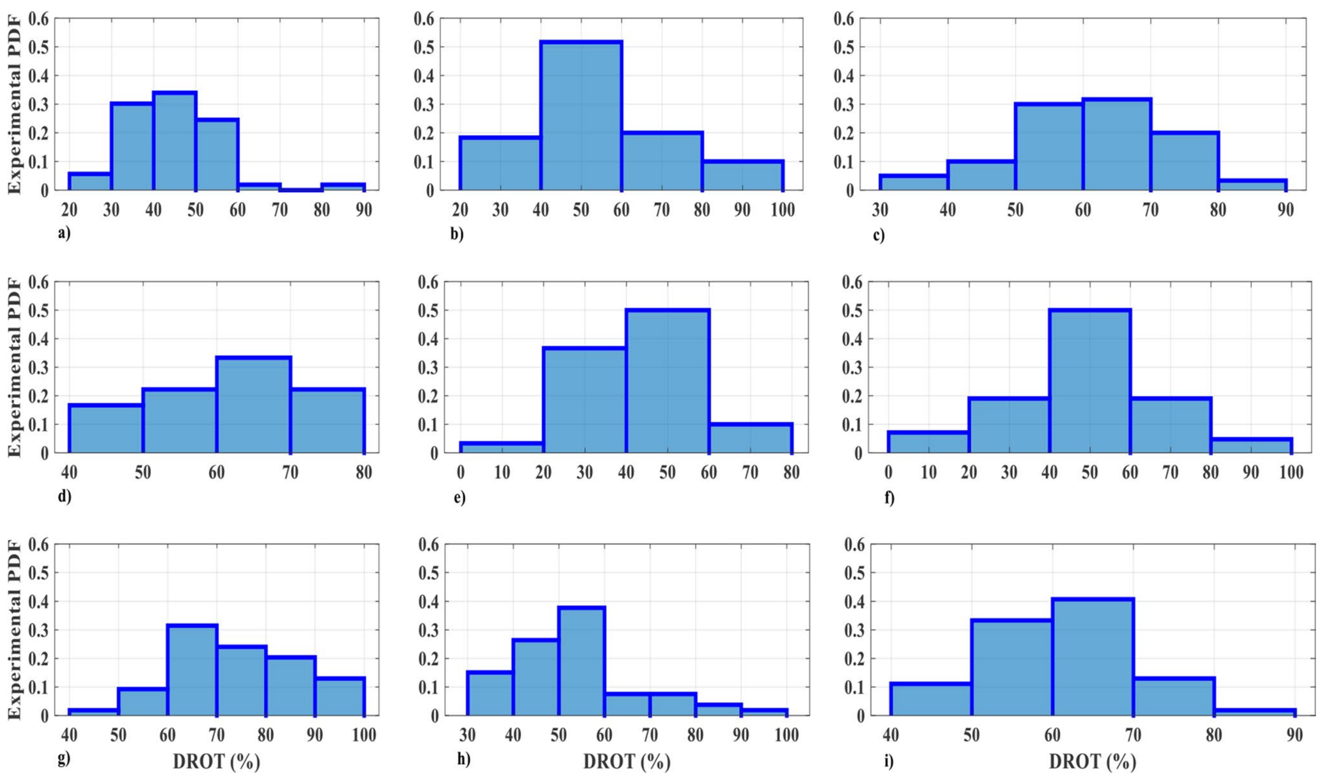

Fig. 5 The EPDFs of the DROT (%) for all stations according to earthquakes from large to small: **a**) E1, **b**) E2, **c**) E3, **d**) E4, **e**) E5, **f**) E6, **g**) E7, **h**) E8 and **i**) E9 and E10

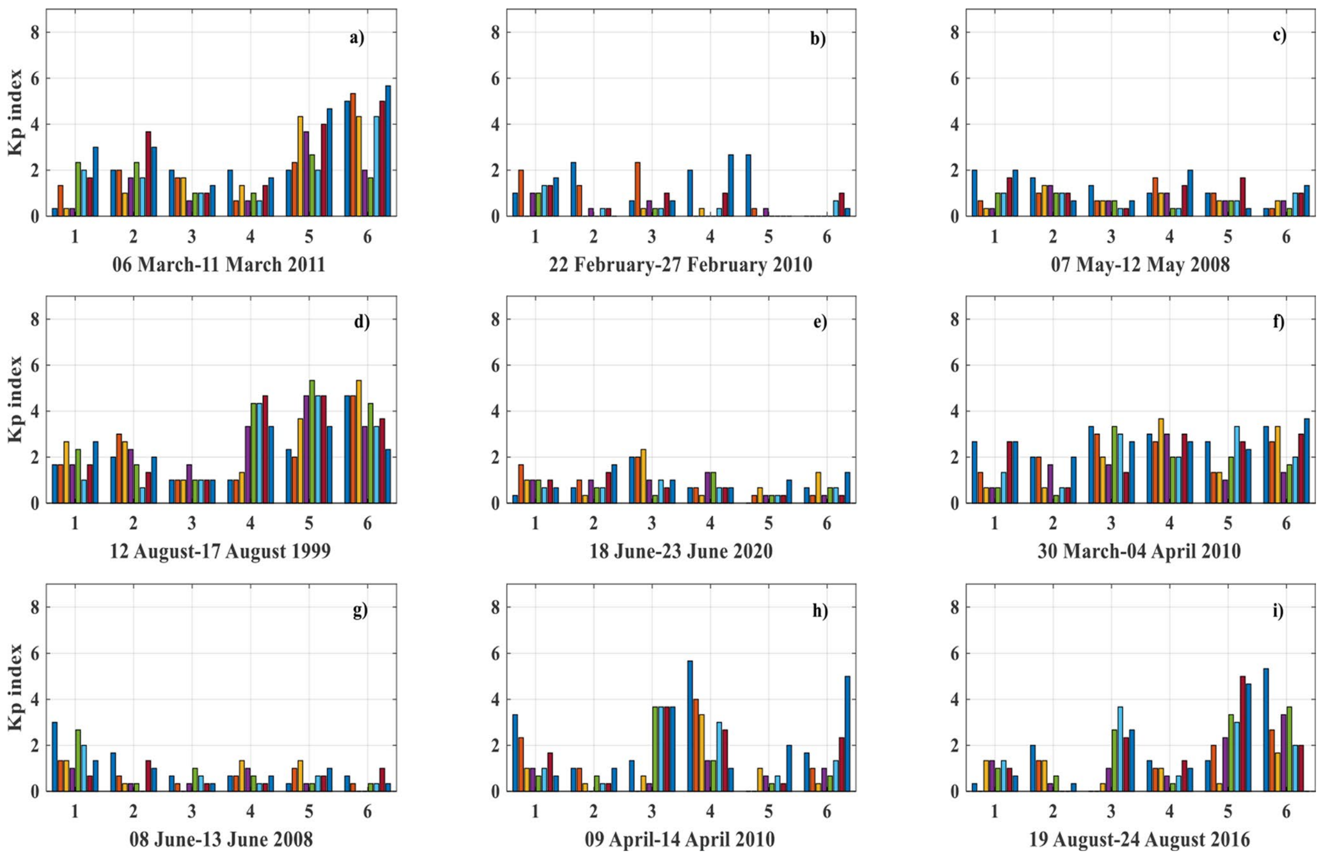

Fig. 6 The Kp values in the days before the earthquakes and the earthquake days for: **a**) E1, **b**) E2, **c**) E3, **d**) E4, **e**) E5, **f**) E6, **g**) E7, **h**) E8 and **i**) E9 and E10 (GFZ, n.d.)

between 40% and 50%, the highest accumulation range in the smallest magnitude earthquakes Mw 6.2 and 5.6 E9 and E10 is between 60% and 70%. This difference may be due to the depth of the earthquake. It is observed that the bin ranges are larger for earthquakes with a magnitude greater than Mw 7.0. In all earthquakes except E4 and E5 earthquakes, the maximum DROT value reaches 90% and above. A considerable amount of the counts of DROT values greater than 70% is also observed in comparison of earthquakes, which has been accepted as an indicator of large-scale ionospheric disturbances. The averages in comparison of earthquakes are in the order of 60%. It is observed that even the accumulation range is between 60% and 70% in the E3 earthquake, where the stations from which data can be provided are very distant (min. 700 km) and in the E4 earthquake, where data can be provided from very few stations (3 stations). Both of these earthquakes are greater than Mw 7.5.

Figure 7 shows the EPDFs of the DROT (%) for all stations starting from the earthquake day, one day, two days, three days, four days and five days before the earthquakes, respectively. When Fig. 7 is compared within itself, it is observed that the maximum accumulation range is between 50% and 60% in all day categories before the earthquake day. It means that there has been medium-scale ionospheric disturbances occurred one day, two days, three days, four days and five days before the earthquakes. On earthquake days, DROT values cluster between 60% and 70%, which is indicator of a large-scale disturbance. The count of DROT values between 50% and 60% decreases as the days move away from the earthquake day. The maximum count of DROT values between 50% and 60% is observed one day before the earthquakes. These results indicate that medium-scale disturbances may occur in the ionosphere in the five days before and during the earthquake days.

To show the effects of the disturbances due to the earthquake and seismic activity on the TEC, DROT values are given in Fig. 8 from one day to six days after the earthquakes, respectively. When Fig. 8 is investigated, it is observed that the disturbances in the TEC continue after the earthquakes and that the disturbances before the earthquakes are caused by seismic activity. Especially two, three and four days after earthquakes, DROT values accumulate between 50% and 80%. Even six days after the earthquake, there appears to be a medium-scale disturbance in the ionosphere.

In studies examining the potential physical mechanisms driving the ionospheric disturbances occurred before the

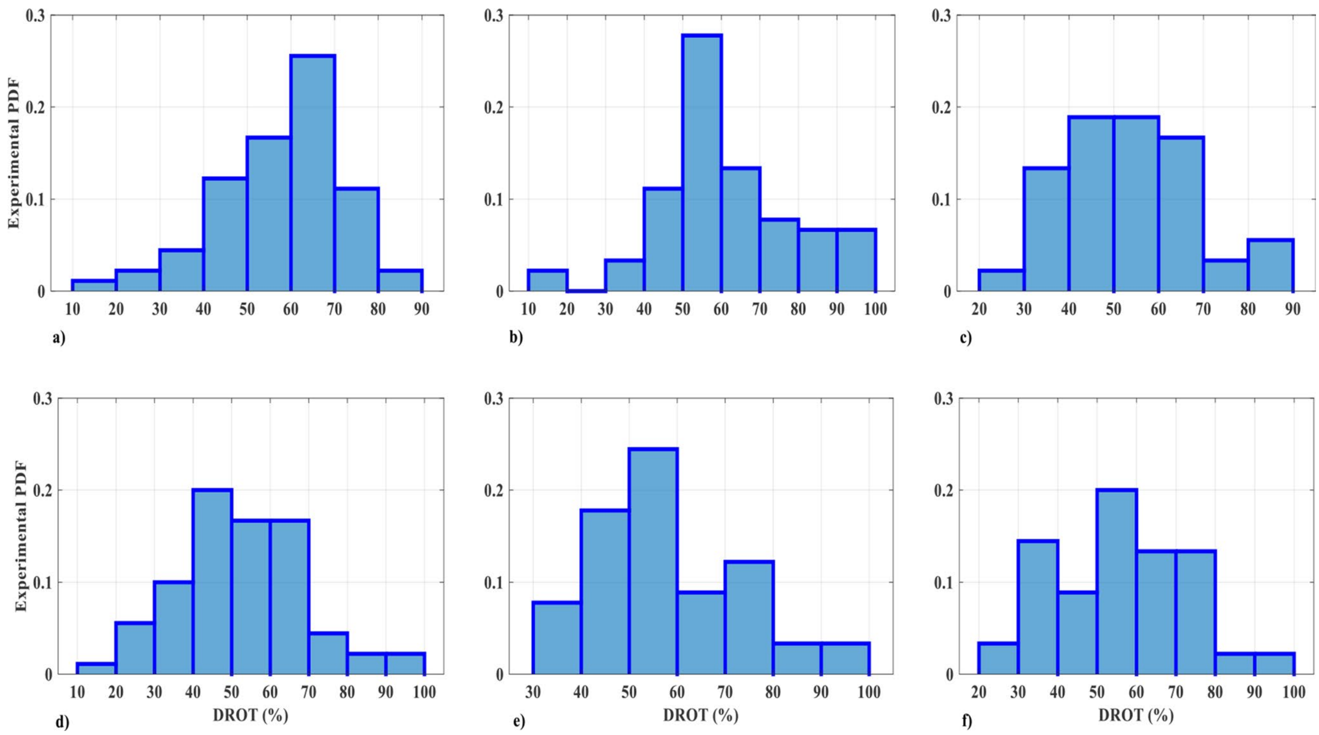

Fig. 7 The EPDFs of the DROT (%) for all stations for the days until the earthquake day: **a**) the earthquakes days, **b**) one day before the earthquakes, **c**) two days before the earthquakes, **d**) three days before the earthquakes, **e**) four days before the earthquakes and **f**) five days before the earthquakes

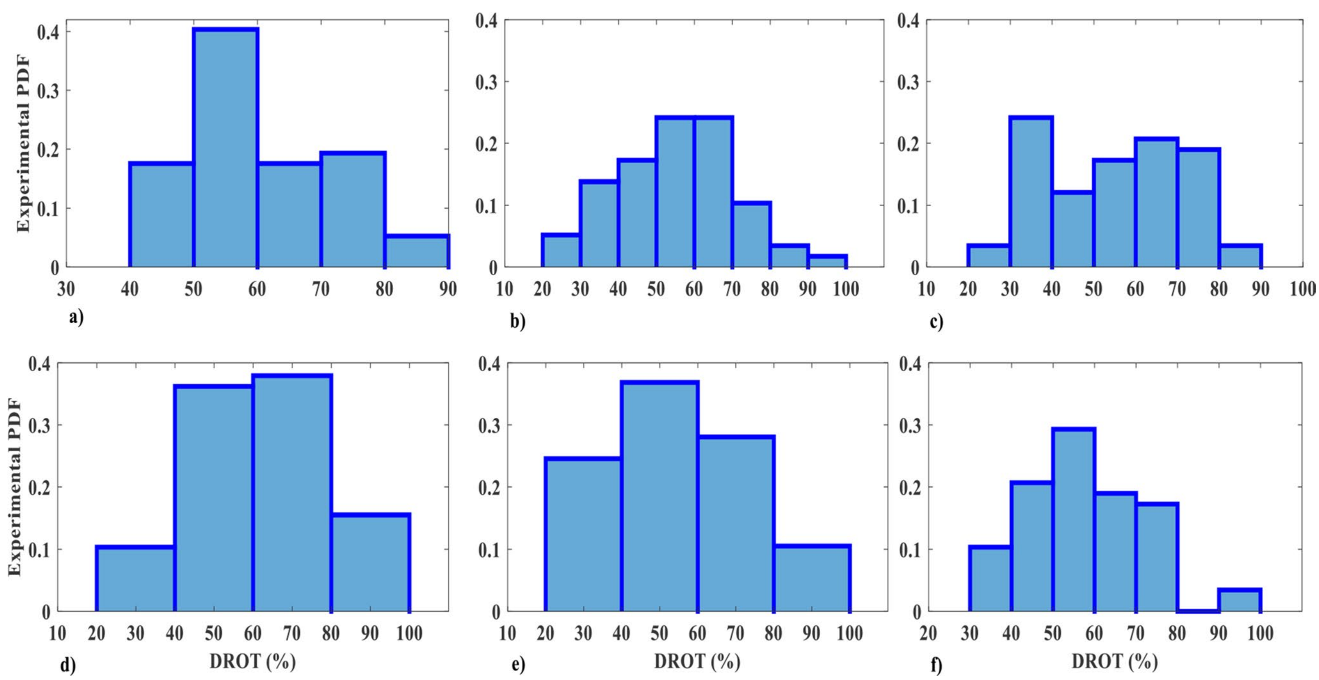

Fig. 8 The EPDFs of the DROT (%) for all stations for: **a**) one day after the earthquakes, **b**) two days after the earthquakes, **c**) three days after the earthquakes, **d**) four days after the earthquakes, **e**) five days after the earthquakes and **f**) six days after the earthquakes

strong earthquakes, primary cause of atmospheric and ionospheric anomalies observed one week to a few days prior to major earthquakes is natural ground radioactivity (Radon along active tectonic faults). Energy can be released in the form of Radon gas or other chemical emissions when stress builds up in the Earth's crust prior to an earthquake. The ionosphere may be impacted by these activities since they may have an impact on the electric fields and conductivity of the atmosphere. Micro fractures in the lithosphere can produce Radon gas, which can ionize air molecules and increase atmospheric conductivity. The electric field is changed by this ionization, and the changes are transmitted upward to the ionosphere (Pulinets & Ouzounov, 2011). In addition, ionospheric conditions may be impacted by the upward propagation of electromagnetic waves produced by piezoelectric or triboelectric phenomena in strained rocks (Freund 2011). Some large earthquakes have been preceded by low-frequency electromagnetic abnormalities, which may be related to ionospheric disturbances (Parrot et al. 2021). Localized electric fields produced by stress buildup in the lithosphere may travel to the ionosphere by convection or conduction. Ionospheric plasma can be changed by localized electric fields through charge redistribution or instabilities. Ionospheric dynamics may be impacted by a direct current that is produced by the redistribution of charges in the crust (Pulinets et al. 1998; Imtiaz and Marchand 2012). Ionospheric conditions may be indirectly altered by variations in atmospheric parameters such as temperature, humidity, and pressure close to the fault zone. Changes in the density of the atmosphere can spread to the ionosphere and change its composition (Ondoh 2009). GPS satellite measurements of TEC frequently reveal significant disturbances before to the strong earthquakes (Liu et al. 2004a, b; Karatay et al. 2010; Pulinets et al. 2005). Integrating data from atmosphere, space-based and ground-based observations is necessary to comprehend pre-earthquake ionospheric disturbances. The interaction of these factors offers a viable foundation for furthering earthquake prediction research, even though none of them can completely account for all observed occurrences.

The persistence of ionospheric disturbances both before and after earthquake events requires careful interpretation to establish a meaningful connection with seismic activity. While our analysis shows medium-scale disturbances (DROT values between 50 and 60%) throughout the observation period, several key features in our data support a specific relationship with seismic events:

1. Temporal evolution pattern: The DROT distribution shows a distinct evolution pattern, with the most pronounced disturbances (60–70%) occurring on earthquake days. This peak in disturbance intensity coinciding with seismic events suggests a direct physical connection rather than random correlation. The gradual build-up of disturbances before the earthquake and their persistence afterward follows a pattern consistent with the mechanics of Lithosphere-Atmosphere-Ionosphere Coupling (LAIC).
2. Intensity variation: Although medium-scale disturbances persist throughout the observation period, there is a notable intensification during and immediately following the seismic events. The clustering of DROT values between 50 and 80% in the two to four days post-earthquake period, compared to the pre-earthquake baseline of 50–60%, indicates an enhancement of ionospheric perturbations linked to seismic activity.
3. Physical mechanism context: The observed post-seismic ionospheric disturbances can be explained by established physical mechanisms. During and after significant seismic events, the release of energy into the atmosphere can trigger Acoustic-Gravity Waves (AGW) that propagate upward and interact with the ionosphere. These interactions can persist for several days due to:

    - Continued aftershock activity maintaining the perturbation.
    - Atmospheric wave dynamics that take time to dissipate.
    - Secondary effects from modified electric fields in the ionosphere.

4. Comparative analysis with background conditions: To strengthen our interpretation, we acknowledge that background ionospheric variability exists due to various sources (solar activity, geomagnetic conditions, etc.). However, the temporal clustering of enhanced disturbances around earthquake events, particularly the shift from 50 to 60% to 60–70% DROT values during seismic activity, suggests a superposition of earthquake-related effects on background variability.
5. Extended duration of effects: The persistence of disturbances up to six days post-earthquake, rather than undermining the seismic connection, actually aligns with previous studies of post-seismic phenomena. The gradual return to background levels follows a pattern consistent with the relaxation time of the LAIC system. This extended duration reflects:

    - The continued release of seismic energy through aftershocks.
    - The time required for atmospheric wave propagation and dissipation.
    - The ionosphere's recovery period following significant perturbations.

This comprehensive analysis suggests that while background ionospheric variability exists, the specific pattern, intensity, and temporal evolution of disturbances observed in our study provides strong evidence for a causal relationship with seismic activity. The persistence of these effects after the main shock is consistent with our current understanding of LAIC mechanisms and the complex nature of post-seismic processes.

In the last group of the study, all stations used within the scope of the study are categorized according to their distance to the epicenters. There are 12 categories ranging from 150 km to 200 km and there are at least two stations in one category. Table 3 shows the 12 categories, distances and stations in each category.

After the stations are categorized according to their distance from the epicenters, the EPDFs of the DROT (%) is calculated for each category. Figure 9 shows the EPDFs of the DROT (%) for each category for six days in the chosen earthquakes demonstrated in Fig. 6; Table 2. When Fig. 9 is examined, it is observed that the accumulation range decreases as the distance to the epicenters increases. While the maximum DROT for stations that are at most 50 km away from the epicenters varies between 60% and 80% (Fig. 9a), the maximum DROT values for stations that are more than 2000 km away from the epicenters center vary between 50% and 60% (Fig. 9l). The maximum accumulation range for stations 350 to 500 km away from the epicenters is between 40% and 70%. When the distance is more than 500 km, the maximum accumulation range is between 30% and 60%. This shows that stations located at most 500 km away from the epicenter are more affected by the earthquake.

Table 3 Distance categories for all stations from near to Far according to the distance from the epicenters

Category	Distance	Stations
C1	d ≤ 50 km	TUBI, MIZU
C2	50 km < d ≤ 200 km	ANTC, BLYT, CONZ, DHLG, IGMI, MIZU, MONP, PIN1,
C3	200 km < d ≤ 350 km	ANKR, CRFP, MEDI, TRAK, TSK2, TSKB, TSK2, TSKB
C4	350 km < d ≤ 500 km	AJAC, BZRG, GENO, GOL2, IENG, MAT1, MATE, MTKA, MTKA, SANT, STK2, USUD, USUD
C5	500 km < d ≤ 650 km	CFAG, GUAT, SOFI, STK2, XIAN,
C6	650 km < d ≤ 800 km	KUNM, LHAZ, NOT1, SMST, SSIA, SMST
C7	800 km < d ≤ 1000 km	COPO, INEG, YSSK, YSSK,
C8	1000 km < d ≤ 1300 km	AIRA, AIRA, COYQ, KUNM, LHAZ, XIAN
C9	1300 km < d ≤ 1500 km	LPGS, MANA, UNSA, URUM
C10	1500 km < d ≤ 1800 km	IQQE, SHAO
C11	1800 km < d ≤ 2000 km	GUAO, TCMS, URUM
C12	d > 2000 km	AREQ, CHAN, CHAN, DAEJ, DAEJ, RDAD, SHAO, SUWN, SUWN, TCMS

Pre-earthquake ionospheric disturbances often known as ionospheric precursors have long been the focus of scientific studies. These disturbances can appear in a variety of ways and be found in a number of ways. As in this study, pre-seismic TEC anomalies, such as variations in electron density, have been documented days to hours in advance of an earthquake in the literature. Although a number of studies in the literature document ionospheric anomalies preceding earthquakes, it is difficult to consider these disturbances as reliable precursors because they are inconsistent for all seismic events. For the researchers, it remains difficult to distinguish between ionospheric disturbances brought on by seismic activity and those brought on by geomagnetic disturbances. For this reason, in this study, the days used for earthquake periods have been chosen as geomagnetically quiet days. The disturbance caused by geomagnetic activity in the ionosphere has been also chosen on separate days for each year used. Consistent with the results of this investigation, it is recommended that ionospheric data be combined with additional physical, geophysical and geological data in order to enhance our comprehension and capacity for future prediction of these disturbances.

Several studies have shown that solar activity has a major impact on ionospheric anomalies with more solar activity frequently resulting in more severe ionospheric disturbances. Several investigations showed that the ionosphere is more susceptible to electron density fluctuations during high solar activity, which might lead to anomalies that could mask other disturbances, such seismic activity (Pulinets and Boyarchuk 2004; Hernández-Pajares et al. 2006). Liu et al. (2004a) highlighted that during periods of heightened solar activity, ionospheric anomalies such as TEC variations and ionospheric tilts can be exacerbated, making it challenging to distinguish between ionospheric disturbances caused by seismic events and those driven by solar-induced variations. As this study and others have shown, the time of year and the solar cycle phase are crucial for understanding the level of ionospheric activity. Latitude is also a significant factor in ionospheric disturbances in the context of TEC anomalies and the propagation of seismic-related disturbances (Zakharov and Chernogor 2024). It is more challenging to distinguish ionospheric disturbances brought on exclusively by seismic occurrences in high-latitude regions because of the greater influence of solar wind and geomagnetic storms. According to studies, geomagnetic disturbances, which are more common in high-latitude regions, may interfere with the detection of TEC anomalies associated with seismic

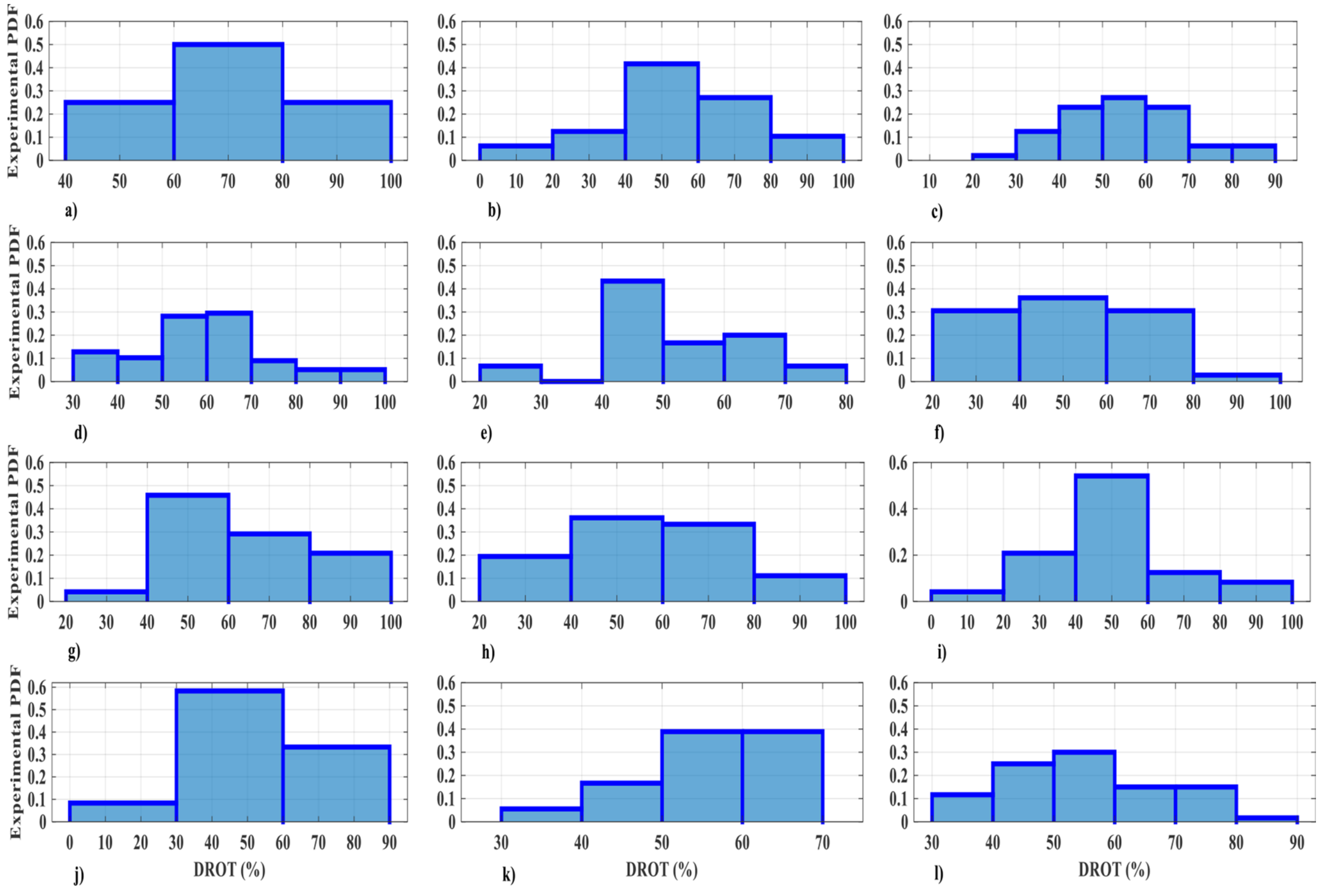

Fig. 9 The EPDFs of the DROT (%) according to the distance of the stations to the epicenters given in Table 2 for: **a**) C1, **b**) C2, **c**) C3, **d**) C4, **e**) C5, **f**) C6, **g**) C7, **h**) C8, **i**) C9, **j**) C10, **k**) C11 and **l**) C12

activity. When examining global ionospheric data, it is crucial to take into account this latitude-dependent variability in ionospheric response.

Ionization decreases at night because the Sun's light no longer directly illuminates the Earth's ionosphere. However, a key factor in determining the ionospheric behavior at these times is the solar illumination boundary, also referred to as the Solar Terminator Height (STH). The STH, which changes during the day, is the line dividing the Earth's dark and sunny sides. Due to residual ionization from the previous day as well as the continued influence of solar wind and geomagnetic activity, the position of the Solar Terminator affects ionospheric parameters, such as TEC, even though the ionosphere is not directly illuminated by the Sun during the night. Therefore, it is crucial to take into account the possible impact of the STH and residual solar activity, in addition to geomagnetic and seismic components during observation periods where disturbances are discovered at night (Rees 1995; Colonna and Tramutoli 2021). The aforementioned factors have the potential to improve the ability to predict ionospheric anomalies and aid in the improvement of seismic disturbance detection.

Conclusion

A possible path for improving our knowledge of earthquake precursors and improving prediction capacity is the spatio-temporal eveluation of pre-earthquake disturbances in the ionosphere. By means of a methodical evaluation of fluctuations in Total Electron Content (TEC), significant anomalies have been detected that are associated with seismic activity in this study. Ten earthquakes with magnitudes between Mw 9.0 and 5.6 have been chosen for the purpose of the study. GPS-TEC estimated as IONOLAB-TEC for five-day earthquake periods, geomagnetic disturbed and quiet periods of the ionosphere have formed the data input of the study. The DROT algorithm, which has been previously used in the literature and reveals the type of ionospheric disturbances, has been applied to the dataset. The findings of the study have been obtained in three groups: temporal and spatial, depending on the magnitude of the earthquake. The temporal approach showed significant TEC oscillations occurred 1–5 days before the earthquakes and a higher frequency of oscillations on the day immediately preceding the each seismic events. The spatial approach revealed clustering up to 500 km away from the epicenters. In the approach depending on the magnitude of the earthquake, large-scale ionospheric disturbances preceded earthquakes with a magnitude greater than Mw 5.6. The results of this study suggest that some ionospheric anomalies in TEC happen in a particular temporal window and in close spatial vicinity to approaching earthquakes. While it remains challenging to differentiate these anomalies due to solar and geomagnetic activities, real-time ionospheric monitoring coupled with sophisticated analytical and signal processing techniques presents interesting avenues to enhance earthquake prediction and preparedness. Future research could explore deeper integrations of ionospheric data with geological and seismic models to develop a more robust predictive framework. Furthermore, expanding datasets to include a broader range of earthquake magnitudes and geographies will allow for greater generalization of findings. Advances in Machine Learning, particularly in anomaly detection and pattern recognition, offer promising tools for automating the identification of pre-earthquake disturbances and reducing false positives. Additionally, collaboration with space agencies and the deployment of next-generation satellites equipped with more precise TEC measurement capabilities could significantly enhance monitoring resolution. Incorporating multi-disciplinary data, including atmospheric and hydrological measurements, will also be crucial to contextualize ionospheric disturbances and distinguish between seismically induced anomalies and those driven by other factors. Lastly, fostering international collaboration for data sharing and model validation can accelerate the development of globally applicable early warning systems.

Acknowledgements The GIM-TEC, Satellite DCB and ephemeris data that are used in computation of IONOLAB-TEC are obtained from IGS Analysis Center of Jet Propulsion Laboratory (JPL) at http://ftp.cddis.gsfc.nasa.gov/pub/gps/products/ionex. Kp and Ap indices are obtained from National Oceanic and Atmospheric Administration (NOAA), U.S. Department of Commerce at http://ftp.swpc.noaa.gov/pub/indices/old_indices/. Earthquake information is obtained from https://earthquake.usgs.gov/earthquakes. Dst indices are obtained from http://wdc.kugi.kyoto-u.ac.jp/. The authors are grateful to anonymous reviewers for their comments and contributions, which have been very helpful and constructive for the authors in improving the paper.

Author contributions SK and FA developed the algorithm, SK and AP applied and performed the algorithm, SK, FA and AP obtained and analyzed the results, SK, FA and AP wrote the manuscript.

Funding Open access funding provided by the Scientific and Technological Research Council of Türkiye (TÜBİTAK).
Not applicable.

Data availability No datasets were generated or analysed during the current study.

Declarations

Ethics approval and consent to participate Not applicable.

Consent for publication Not applicable.

Competing interests The authors declare no competing interests.

References

Akyol AA, Arikan O, Arikan F (2020) A machine Learning-Based detection of earthquake precursors using ionospheric data. Radio Sci 55(11):1–21. https://doi.org/10.1029/2019RS006931

Arikan F, Erol CB, Arikan O (2003) Regularized Estimation of vertical total electron content from global positioning system data. Space Phys 108(A12):1–20. https://doi.org/10.1029/2002JA009605

Arikan F, Erol C, Arikan O (2004) Regularized Estimation of vertical total electron content from GPS data for a desired time period. Radio Sci 39(6):1–10. https://doi.org/10.1029/2002JA009605

Arikan F, Nayir H, Sezen U, Arikan O (2008) Estimation of single station interfrequency receiver bias using GPS-TEC. Radio Sci 43(4):1–13. https://doi.org/10.1029/2007RS003785

Arikan F, Efendi E, Cinar A, Karatay S (2017) Investigation of seasonal trend anomalies in midlatitude ionosphere using DROT. Second Variability of the Sun and Its Terrestrial Impact General Symposium (VarSITI-2017), Irkutsk, Russia, 10–15 July 2017

Basu S, Groves K, Quinn J, Doherty P (1999) A comparison of TEC fluctuations and scintillations at ascension Island. J Atmos Solar Terr Phys 61(16):1219–1226. https://doi.org/10.1016/S1364-6826(99)00052-8

Bolt BA (1964) Seismic air waves from the great 1964 Alaskan earthquake. Nature 202:1095–1096. https://doi.org/10.1038/2021095a0

Budak C, Gider V (2023) LSTM based forecasting of the next day's values of ionospheric total electron content (TEC) as an earthquake precursor signal. Earth Sci Inf 16:2323–2337. https://doi.org/10.1007/s12145-023-01027-2

Budak C, Karatay S, Erken F, Cinar A (2024) Classification of the ionospheric disturbances caused by geomagnetic and seismic activity with K-Nearest neighbors algorithm. Wireless Pers Commun 134:1551–1569. https://doi.org/10.1007/s11277-024-10965-z

Carbone V, Piersanti M, Materassi M, Battiston R, Lepreti F, Ubertini P (2021) A mathematical model of lithosphere–atmosphere coupling for seismic events. Sci Rep 11:1–12. https://doi.org/10.1038/s41598-021-88125-7

Carmo CS, Denardini CM, Figueiredo CAOB, Resende LCA, Picanço GAS, Barbosa Neto PF, Nogueira PAB, Moro J, Chen SS (2021) Evaluation of different methods for calculating the ROTI index

over the Brazilian sector. Radio Sci 56(8):1–12. https://doi.org/10.1029/2020RS007140
Cherniak I, Zakharenkova I, Krankowski A (2014) Approaches for modeling ionosphere irregularities based on the TEC rate index. Earth Planets and Space 66(165):1–5. https://doi.org/10.1186/s40623-014-0165-z
Colonna R, Tramutoli V (2021) A new model of solar illumination of Earth's atmosphere during Night-Time. Earth 2(2):191–207. https://doi.org/10.3390/earth2020012
Colonna R, Filizzola C, Genzano N, Lisi M, Tramutoli V (2023) Optimal setting of Earthquake-Related ionospheric TEC (Total electron Content) anomalies detection methods: Long-Term validation over the Italian region. Geosciences 13(5):1–48. https://doi.org/10.3390/geosciences13050150
Davidenko DV, Pulinets SA (2019) Deterministic variability of the ionosphere on the eve of strong (M≥6) earthquakes in the regions of Greece and Italy according to Long-Term measurements data. Geomag Aeron 59:493–450. https://doi.org/10.1134/S001679321904008X
Davies K (1990) Ionospheric radio. Peter Peregrinus Ltd, London
Donn WL, Posmentier ES (1964) Ground-coupled air waves from the great Alaskan earthquake. J Phys Res 69(24):5357–5361. https://doi.org/10.1029/JZ069i024p05357
Efendi E, Arikan F (2017) A fast algorithm for automatic detection of ionospheric disturbances: DROT. Adv Space Res 59(12):2923–2933. https://doi.org/10.1016/j.asr.2017.03.018
Eshkuvatov HE, Ahmedov BJ, Tillayev YA, Tariq MA, Shah MA, Liu L (2023) Ionospheric precursors of strong earthquakes observed using six GNSS stations data during continuous five years (2011–2015). Geodesy Geodyn 14(1):65–69. https://doi.org/10.1016/j.geog.2022.04.002
Freund F (2011) Pre-earthquake signals: underlying physical processes. J Asian Earth Sci 41(4–5):383–400. https://doi.org/10.1016/j.jseaes.2010.03.009
GFZ n.d. Geo Forschungs Zentrum. [Online] Available at: https://kp.gfz-potsdam.de/en/data#c134 [Accessed 20 11 2024]
Ghimire BD, Chapagain NP (2022) Geomag Aeron 62:460–473. https://doi.org/10.1134/S0016793222040041. Ionospheric Anomalies Due to Nepal Earthquake-2015 as Observed from GPS-TEC Data
Ghosh D, Deb A, Sengupta R (2009) Anomalous radon emission as precursor of earthquake. J Appl Geophys 69(2):67–81. https://doi.org/10.1016/j.jappgeo.2009.06.001
Gurbuz G, Akgul V, Kutoglu SH (2023) Comprehensive ionospheric precursor analysis of selected mw≥7 earthquakes. Environ Earth Sci 82:1–11. https://doi.org/10.1007/s12665-023-11136-2
Hargreaves JK (1992) The Solar-Terrestrial environment: an introduction to Geospace – the science of the terrestrial upper atmosphere, ionosphere, and magnetosphere. Cambridge University Press, Cambridge
Hayakawa M, Izutsu J, Schekotov A, Yang S-S, Solovieva M, Budilova E (2021) Lithosphere–Atmosphere–Ionosphere coupling effects based on multiparameter precursor observations for February–March 2021 earthquakes (M~7) in the offshore of Tohoku area of Japan. Geosciences 11(11):1–29. https://doi.org/10.3390/geosciences11110481
He L, Guo C, Yue Q, Zhang S, Qin Z, Zhang J (2023) A novel ionospheric disturbance index to evaluate the global effect on BeiDou navigation satellite system signal caused by the moderate geomagnetic storm on May 12, 2021. Sensors 23(3):1–18. https://doi.org/10.3390/s23031183
Hernández-Pajares M, Juan JM, Sanz J (2006) Medium-scale traveling ionospheric disturbances affecting GPS measurements: Spatial and Temporal analysis. J Geophys Research: Space Phys 111(A7):1–13. https://doi.org/10.1029/2005JA011474
Hirooka S, Hattori K, Nishihashi M, Takeda T (2011) Neural network based tomographic approach to detect earthquake-related ionospheric anomalies. Nat Hazards Earth Syst Sci 11(8):2341–2353. https://doi.org/10.5194/nhess-11-2341-2011
Hirshberg J, Currie RG, Breiner S (1967) Long period geomagnetic fluctuations after the 1964 Alaskan earthquake. Earth Planet Sci Lett 3(1967–1968):426–428. https://doi.org/10.1016/0012-821X(67)90072-6
Igarashi G, Saeki S, Takahata N, Tasaka S, Sasaki Y, Takahashi M, Sano Y (1995) Ground-Water radon anomaly before the Kobe earthquake in Japan. Science 269(5220):60–61. https://doi.org/10.1126/science.269.5220
Imtiaz N, Marchand R (2012) Modeling of ionospheric magnetic field perturbations induced by earthquakes. J Geophys Research: Space Phys 117(A4):1–10. https://doi.org/10.1029/2011JA017475
Karatay S (2020) Detection of the ionospheric disturbances on GPS-TEC using differential rate of TEC (DROT) algorithm. Adv Space Res 65(10):2372–2390. https://doi.org/10.1016/j.asr.2020.01.042
Karatay S, Gul SE (2023) Prediction of GPS-TEC on mw>5 earthquake days using bayesian regularization backpropagation algorithm. IEEE Geosci Remote Sens Lett 20:1–5. https://doi.org/10.1109/LGRS.2023.3262028
Karatay S, Arikan F, Arikan O (2010) Investigation of total electron content variability due to seismic and geomagnetic disturbances in the ionosphere. Radio Sci 45(5):1–12. https://doi.org/10.1029/2009RS004313
Kelley MC (1989) The Earth's ionosphere plasma physics and electrodynamics. Academic, Cambridge
Khan F, Khattak SA, Wazir Z, Waqas M (2021) Spatial distribution of radon concentrations in Balakot-Bagh (B–B) fault line and adjoining areas, lesser Himalayas, North Pakistan. Environ Earth Sci 80:1–6. https://doi.org/10.1007/s12665-021-09569-8
King C-Y (1986) Gas geochemistry applied to earthquake prediction: an overview. J Geophys Research: Solid Earth 91(B12):12269–12281. https://doi.org/10.1029/JB091iB12p12269
Koroglu M, Arikan F (2018a) Classification of Ionospheric Irregularities over Turkey in 2012 Using DROT on STEC, 42nd COSPAR Scientific Assembly, Pasadena, USA, 14–22 July 2018
Koroglu M, Arikan F (2018b) Directional and time analysis of Wave-like ionospheric disturbances over Turkey using near real time indicator DROT, URSI AT-RASC, Gran Canaria, Spain, 28 May-1 June 2018
Koroglu M, Arikan F (2020) Spatio-temporal analysis of ionospheric disturbances for ground based augmentation systems over a mid-latitude region. Adv Space Res 65(9):2099–2118. https://doi.org/10.1016/j.asr.2019.10.024
Kouris S, Polimeris K, Cander L (2006) Specifications of TEC variability. Adv Space Res 37(5):983–1004. https://doi.org/10.1016/j.asr.2005.01.102
Krankowski A, Shagimuratov I, Baran L, Ephishov I, Tepenitzyna N (2006) The occurrence of Polar cap patches in TEC fluctuations detected using GPS measurements in Southern hemisphere. Adv Space Res 38(11):2601–2609. https://doi.org/10.1016/j.asr.2005.12.006
Larkina VI, Migulin VV, Molchanov OA, Kharkov IP, Inchin AS, Schvetcova VB (1989) Some statistical results on very low frequency radiowave emissions in the upper ionosphere over earthquake zones. Phys Earth Planet Inter 57(1–2):100–109. https://doi.org/10.1016/0031-9201(89)90219-7
Liu JY, Chen YI, Pulinets SA, Tsai YB, Chuo YJ (2000) Seismo-ionospheric signatures prior to M≥6.0 Taiwan earthquakes. Geophys Res Lett 27(19):3113–3116. https://doi.org/10.1029/2000GL011395
Liu JY, Chen YI, Jhuang HK, Lin YH (2004a) Ionospheric foF2 and TEC anomalous days associated with M>=5.0 earthquakes in Taiwan during 1997–1999. Terr Atmospheric Ocean Sci 15(3):371–383. https://doi.org/10.3319/TAO.2004.15.3.371(EP)

Liu JY, Chuo YJ, Shan SJ, Tsai YB, Chen YI, Pulinets SA, Yu SB (2004b) Pre-earthquake ionospheric anomalies registered by continuous GPS TEC measurements. Ann Geophys 22(5):1585–1593. https://doi.org/10.5194/angeo-22-1585-2004

Liu JY, Chang FY, Chen YI, Chang LC, Wen YC, Wu TY, Chao CK (2023) Pre-earthquake ionospheric anomalies and ionospheric storms observed by FORMOSAT-5/AIP and GIM TEC. Surv Geophys 45:577–602. https://doi.org/10.1007/s10712-023-09807-7

Molchanov OA, Hayakawa M, Rafalsky VA (1995) Penetration characteristics of electromagnetic emissions from an underground seismic source into the atmosphere, ionosphere, and magnetosphere. J Geophys Research: Space Phys 100(A2):1691–1712. https://doi.org/10.1029/94JA02524

Molchanov O, Fedorov E, Schekotov A, Gordeev E, Chebrov V, Surkov V, Rozhnoi A, Andreevsky S, Iudin D, Yunga S, Lutikov A, Hayakawa M, Biagi PF (2004) Lithosphere-atmosphere-ionosphere coupling as governing mechanism for preseismic short-term events in atmosphere and ionosphere. Nat Hazards Earth Syst Sci 4:757–767. https://doi.org/10.5194/nhess-4-757-2004

Nayak K, Lopez-Urias C, Romero-Andrade R, Sharma G, Guzman-Acevedo GM, Trejo-Soto ME (2023) Ionospheric total electron content (TEC) anomalies as earthquake precursors: unveiling the geophysical connection leading to the 2023 Moroccan 6.8 Mw earthquake. Geosciences 13(11):1–17. https://doi.org/10.3390/geosciences13110319

Nayir H, Arikan F, Arikan O, Erol CB (2007) Total electron content Estimation with Reg-Est. J Geophys Research: Space Phys 112(A11):1–11. https://doi.org/10.1029/2007JA012459

NOAA n.d. National Oceanic and Atmospheric Administration. [Online] Available at: https://www.noaa.gov/ [Accessed 20 11 2024]

Ondoh T (2009) Investigation of precursory phenomena in the ionosphere, atmosphere and groundwater before large earthquakes of M > 6.5. Adv Space Res 43(2):214–223. https://doi.org/10.1016/j.asr.2008.04.003

Parrot M, Tramutoli V, Liu TJY, Pulinets S, Ouzounov D, Genzano N, Lisi M, Hattori K, Namgaladze A (2021) Atmospheric and ionospheric coupling phenomena associated with large earthquakes. Eur Phys J Special Top 230:197–225. https://doi.org/10.1140/epjst/e2020-000251-3

Pi X, Mannucci AJ, Lindqwister UJ, Ho CM (1997) Monitoring of global ionospheric irregularities using the worldwide GPS network. Geophys Res Lett 24(18):2283–2286. https://doi.org/10.1029/97GL02273

Pulinets S, Boyarchuk K (2004) Ionospheric precursors of earthquakes. Springer Berlin, Heidelberg

Pulinets S, Ouzounov D 2(011) Lithosphere–Atmosphere–Ionosphere Coupling (LAIC) model – An unified concept for earthquake precursors validation. Journal of Asian Earth Sciences 41(4–5):371–382. https://doi.org/10.1016/j.jseaes.2010.03.005

Pulinets SA, Khegai VV, Boyarchuk KA, Lomonosov AM (1998) The atmospheric electric field as a source of variability in the ionosphere. Phys Usp 41(5):515–522. https://doi.org/10.1070/PU1998v041n05ABEH000399

Pulinets SA, Gaivoronska TB, Contreras AL, Ciraolo L (2004) Correlation analysis technique revealing ionospheric precursors of earthquakes. Nat Hazards Earth Syst Sci 4(5/6):697–702. https://doi.org/10.5194/nhess-4-697-2004

Pulinets SA, Contreras AL, Bisiacchi-Giraldi G, Ciraolo L (2005) Total eletron content variations in the ionosphere before the colima, Mexico, earthquake of 21 January 2003. Geofisica Int 44(4):369–377. https://doi.org/10.22201/igeof.00167169p.2005.44.4.237

Rees D (1995) Observations and modelling of ionospheric and thermospheric disturbances during major geomagnetic storms: A review. J Atmos Terr Phys 57(12):1433–1457. https://doi.org/10.1016/0021-9169(94)00142-B

Row RV (1966) Evidence of long-period acoustic-gravity waves launched into the F region by the Alaskan earthquake of March 28, 1964. J Phys Res 71(1):343–345. https://doi.org/10.1029/JZ071i001p00343

Sezen U, Arikan F, Arikan O, Ugurlu O, Sadeghimorad A (2013) Online, automatic, near-real time Estimation of GPS-TEC: IONOLAB-TEC. Space Weather 11(5):297–305. https://doi.org/10.1002/swe.20054

Shah M, Ahmed A, Ehsan M, Khan M, Tariq MA, Calabia A, Rahman Z (2020) Total electron content anomalies associated with earthquakes occurred during 1998–2019. Acta Astronaut 175:268–276. https://doi.org/10.1016/j.actaastro.2020.06.005

Su J, Chen H (2023) Study on the mechanism of atmospheric electric field anomalies before earthquakes. Results Geophys Sci 15:1–5. https://doi.org/10.1016/j.ringps.2023.100060

Tachema A (2024) Identifying pre-seismic ionospheric disturbances using space geodesy: A case study of the 2011 Lorca earthquake (Mw 5.1), Spain. Earth Sci Inf 17:2055–2071. https://doi.org/10.1007/s12145-024-01272-z

Tao D, Cao J, Battiston R, Li L, Ma Y, Liu W, Zhima Z, Wang L, Dunlop MW (2017) Seismo-ionospheric anomalies in ionospheric TEC and plasma density before the 17 July 2006 M7.7 South of Java earthquake. Ann Geophys 35:589–598. https://doi.org/10.5194/angeo-35-589-2017

Trique M, Richon P, Perrier F, Avouac JP, Sabroux JC (1999) Radon emanation and electric potential variations associated with transient deformation near reservoir lakes. Nature 399:137–141. https://doi.org/10.1038/20161

Tsuchiya M, Nagaham H, Muto J, Hirano M, Yasuoka Y (2024) Detection of atmospheric radon concentration anomalies and their potential for earthquake prediction using random forest analysis. Sci Rep 14:1–9. https://doi.org/10.1038/s41598-024-61887-6

USGS n.d. United States Geological Survey. [Online] Available at: https://www.usgs.gov/programs/earthquake-hazards/earthquakes [Accessed 20 11 2024]

WDC n.d. WDC for Geomagnetism, Kyoto. [Online] Available at: https://wdc.kugi.kyoto-u.ac.jp/dstae/index.html [Accessed 20 11 2024]

Weaver PF, Yuen PC, Prolss GW, Furumoto AS (1970) Acoustic coupling into the ionosphere from seismic waves of the earthquake at Kurile Islands on August 11, 1969. Nature 226:1239–1241. https://doi.org/10.1038/2261239a0

Wilken V, Kriegel M, Jakowski N, Berdermann J (2018) An ionospheric index suitable for estimating the degree of ionospheric perturbations. J Space Weather Space Clim 8(A19):1–9. https://doi.org/10.1051/swsc/2018008

Xie T, Chen B, Wu L, Dai W, Kuang C, Miao Z (2021) Detecting Seismo-Ionospheric anomalies possibly associated with the 2019 Ridgecrest (California) earthquakes by GNSS, CSES, and swarm observations. J Geophys Research: Space Phys 126(9):1–27. https://doi.org/10.1029/2020JA028761

Yao YB, Chen P, Zhang S, Chen JJ, Yan F, Peng WF (2012) Analysis of pre-earthquake ionospheric anomalies before the global M = 7.0 + earthquakes in 2010. Nat Hazards Earth Syst Sci 12(3):575–585. https://doi.org/10.5194/nhess-12-575-2012

Zakharov IG, Chernogor LF (2024) Global and local effects of seismic activity in the ionosphere. Kinematics Phys Celestial Bodies 40:214–224. https://doi.org/10.3103/S0884591324040068

Publisher's note Springer Nature remains neutral with regard to jurisdictional claims in published maps and institutional affiliations.